Journal of Applied Fluid Mechanics, Vol. 9, No. 5, pp. 2545-2557, 2016.
Available online at www.jafmonline.net, ISSN 1735-3572, EISSN 1735-3645.
DOI: 10.18869/acadpub.jafm.68.236.25552

Numerical Analysis of Turbocharger's Bearing using Dynamic Mesh

J. Moradi Cheqamahi, M. Nili-Ahmadabadi, S. Akbarzadeh† and M. Saghafian

Department of Mechanical Engineering1, Isfahan University of Technology, Isfahan, Iran 84156-83111

†*Corresponding Author Email:s.akbarzadeh@cc.iut.ac.ir*

(Received August 31, 2015; accepted December 8, 2015)

ABSTRACT

Journal bearings are widely used in different machineries. Reynolds equation is the governing equation to predict pressure distribution and load bearing capacity in journal bearings. There are many analytical and numerical methods for solving this equation. The main disadvantage of these methods is their inability to analyze complex geometries. In this paper, a comprehensive method based on dynamic mesh method is developed to solve the conservation equations of mass, momentum and energy. This method has smaller error compared to other techniques. To verify the accuracy of this method, the bearings with different length to diameter ratios are analytically and numerically analyzed under different loads and compared with each other. In continue, the turbocharger's bearing is numerically simulated and the effects of rotational speed change are studied. Finally, the turbocharger's bearing with four axial grooves are simulated. The simulations results show that adding grooves to the turbocharger's bearing causes the bearing eccentricity ratio and lubricant flow rate to increase and the attitude angle, rate of temperature rise and frictional torque to decrease.

Keywords: Journal bearing; Turbocharger's bearing; Analytical solution; Dynamic mesh; Axial groove.

NOMENCLATURE

A_L	long-bearing-eccentricity-ratio function in log scale	S	Sommerfeld number
A_S	short-bearing eccentricity-ratio function in log scale	s	location of journal
C_0, C_1...	coefficients of finite analytic equation	T	temperature
C_L	long-bearing-model correction factor	T_{ave}	lubricant average temperature
C	bearing clearance	U	tangential surface velocity of journal
C_p	specific heat of lubricant	$\bar{u}$	mesh displacement velocity
D	journal diameter	u	velocity of fluid flow
D_i	diameter of oil input holes	W	load-bearing capacity
F_{Aero}	the force caused by fluid on journal	$\bar{W}$	dimensionless load
f	Coefficient of Friction	X	slenderness ratio in log scale
$f_L(\varepsilon)$	long-bearing-eccentricity-ratio function	X_L	long bearing mesh point in log scale
$f_S(\varepsilon)$	short-bearing-eccentricity-ratio function	X_S	short bearing mesh point in log scale
h	film thickness; enthalpy	x	circumferential coordinate of journal
h_m	fluid film thickness at the location in which maximum pressure occurs	Y	dimensionless load in log scale
L	bearing length	y	axial coordinate of bearing
m	mass	γ	diffusion coefficient
N	journal rotational speed	ΔT	lubricant temperature rise
P	bearing pressure distribution	ε	bearing eccentricity ratio
Q	oil flow rate	θ	circumferential angle of journal
R	journal radius	μ	lubricant viscosity
		τ	shear stress
		ρ	lubricant density
		ω	journal rotational speed
		φ	attitude angle

1. INTRODUCTION

Industrial machineries with high speed and high loads, such as steam turbines, centrifugal compressors, pumps and motors, utilize journal bearings as rotor supports. One of the main applications of journal bearings is in turbochargers such as internal combustion engines. They are used to increase the engine's efficiency and power output by forcing extra air into the combustion chamber. In latest applications, turbochargers are used in aircraft and gas turbines as well.

Journal bearing is a type of bearing that cover some or all of a rotary shaft and bears the applied radial loads. Usually, its performance is based on the properties of the lubricant film that is formed in the converged gap between shaft and bearing. Fig. 1 illustrates a schematic of a journal bearing from top view and side view.

In many journal bearings, the lubrication regime is hydrodynamic in which the load bearing surfaces are completely separated by a relatively thick lubricant film Shigley (2003).

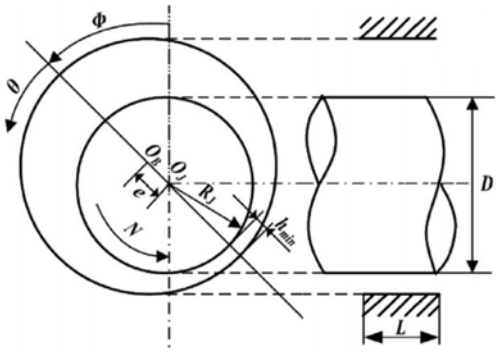

Fig. 1. View of journal bearing with a suitable details.

The issue of journal bearing and its performance dates back to 19th century. Reynolds (1886) developed the governing equation in a bearing-type geometry using simplifying assumptions based on the mass and momentum conservation equations. Using Reynolds equation, one can achieve pressure distribution in the oil film in hydrodynamic lubrication regime. Sommerfeld (1904)analyzed Reynolds equation with the assumption of unlimited length bearing regardless of pressure variations in axial direction. Gümbel (1921) ignored the negative pressures to solve Reynolds equation for infinite bearings. Christopherson (1941) solved Reynolds equation using finite difference method. Dubois and Ocvirk (1953) analytical solved Reynolds equation with the assumption of short bearing regardless of pressure variation in circumferential direction.Raimondi and Boyd (1958) solved Reynolds equation for journal bearings using finite difference method.

Tao *et al.* (2003)performed numerical simulation for lubrication of the connecting rod bearing. The simulations were performed for several known eccentricity ratios. In a study, Hydrodynamic parameters of infinitely short approximation bearing with a circumferential groove located in the middle of the bearing were predicted by Naïmi *et al.* (2010). In a work by Deligant *et al.* (2011) computational fluid dynamic model to predict turbocharger's bearing performances was provided and the frictional power was calculated. This simulation was conducted for various values of eccentricity ratio. Lin *et al.* (2013)considered the journal bearing's performance using fluid-structure interaction analysis. They studied the effect of temperature's deviation and cavitation. In a recent researches by Gao *et al.* (2014) the plain journal bearing under hydrodynamic lubrication by water was analyzed numerically. The effect of using water instead of oil and eccentricity ratio's deviation on other parameters was considered.

Chauhan *et al.* (2014) considered the effect of variation of pressure and temperature on the lubricant film. Thermo-hydrodynamic analysis has been conducted for a particular eccentricity and rotational speed. Kumar and Ganapathi (2015) analyzed the hydrodynamic plain journal bearing using fluid structure interaction technique. They focused on the modeling of journal bearings for different values of eccentricity ratios and simulations were carried out to determine the pressure, stress, and deformation of plain journal bearing by CFD fluid structure interaction approach. Gao *et al.* (2015) in another work presented a new bearing bush, with a transition-arc structure, which is favorable for increasing hydrodynamic load-carrying capacity for water-lubricant bearings. Hydrodynamic load-carrying capacity was calculated by means of three-dimensional computational fluid dynamics analysis. Several variants of a journal bearing with a transition-arc structure of different dimensions were analyzed, while the radial clearance of the bearing, eccentricity ratio and the velocity of the journal remained constant. The results showed that observable changes were found in hydrodynamic load-carrying capacity of a water-lubricated journal bearing.

However, there are many numerical and analytical methods for the analysis of journal bearing's hydrodynamic lubrication. Most of analytical solutions are solved using simplifying assumption of the Reynolds equation. Two extreme cases of infinitely short approximation bearing and infinitely long one are solved by neglecting specific terms in the Reynolds equation. For finite width bearings, however, there is no analytical method. The main problem with all of these methods such as the finite difference method is its inability in handling complex geometries of journal bearing. Recently, it has been proved that journal bearings with axial grooves have better performance compared to the other ones. No analytical solution, however, is available to solve the flow inside such geometries.

An axial groove is useful for distributing the oil over the whole bearing and control the oil temperature consequently. Using grooved bearing is a smart idea in turbocharger bearing due to the high

temperature and high shaft speed. Due to the complicated geometry of the grooved bearings, very few analyses have been done using CFD scheme. Most of these analyses correspond to plain bearings in grooved state and for a specific eccentricity ratio. For example Pai *et al*. (2001) analyzed the fluid flow in a journal bearing with three equi-spaced axial grooves which was supplied with water from one end of the bearing using computational fluid dynamics. Wu *et al*. (2015) studied the flow field of an open grooved two-disc system. The system included a rotating finite disc and a stationary finite disc. The rotating disc had radial grooves. The numerical results for the air–oil two-phase flow inside the open grooved two-disc system are calculated using CFD methods.

Many engineering devices have dynamic components and hence, their computational models are no longer fixed in space and time. In these cases, dynamic mesh method is often used to analyze their motion or unsteady fluid dynamics around/inside them. In other words, dynamic mesh refers to situations in which the computational grid changes dynamically during the run of CFD simulation. This opens up the possibility to simulate flows where the geometry changes with time (Fluent (2009). In all fluid solid interaction simulations, dynamic mesh technique is needed. Some examples of dynamic mesh applications are as follow. Zhang *et al.* (2010) calculated the hydrodynamic coefficients of an underwater vehicle using dynamic mesh technique. Dumont *et al.* (2004) presented a 2D numerical model of the aortic valve hemo-dynamics, making use of dynamic mesh.

In all researches related to flow solution inside journal bearings, dynamic mesh technique has not been used for evaluating eccentricity ratio. In this paper, dynamic mesh method is applied to simulate flow inside the turbocharger's journal bearing with relatively complex geometry. In this method, the equations of momentum, continuity and mesh deformation are solved to obtain the unsteady flow field simultaneous with changing the geometry and mesh. Higher accuracy and its ability to predict the performance of bearings with complex geometries are advantages of dynamic mesh method. First, to verify the accuracy of dynamic mesh method, short, long and finite length bearing are analyzed using both analytical and dynamic mesh method and then, the obtained results are compared with each other. This method, however, has the disadvantage of being time-consuming to solve. After ensuring the accuracy of dynamic mesh method, turbocharger bearing with four axial grooves is analyzed using CFD method and dynamic mesh technique.

2. SIMULATION

In this research, both analytical and dynamic mesh method are used for simulation of journal bearing fluid flow. It is worth noting that the analytical solution is used here to be compared with the dynamic mesh solution for simple geometries. A brief description of these methods is given below.

2.1 Analytical Solution of a Journal Bearing

Analytical solutions for different length-to-diameter ratios of bearings are presented in this section. Process of obtaining these equations is shown in Fig. 2:

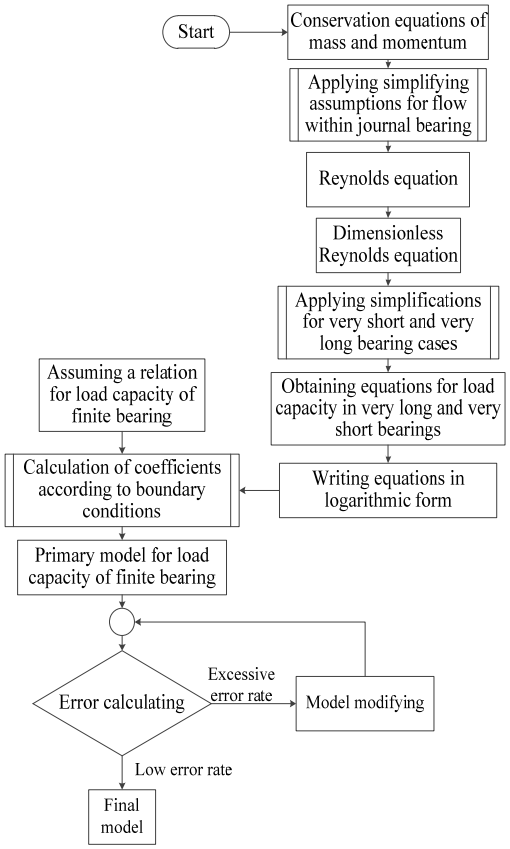

Fig. 2. Analytical solution process.

The main equation governing the flow within a journal bearing is the Reynolds equation for steady-state and incompressible case. Assuming a Newtonian behavior:

$$\frac{\partial}{\partial x}\left(\frac{h^3}{12\mu}\frac{\partial P}{\partial x}\right)+\frac{\partial}{\partial y}\left(\frac{h^3}{12\mu}\frac{\partial P}{\partial y}\right)=\frac{1}{2}U\frac{\partial h}{\partial x} \quad (1)$$

Dimensionless form of Reynolds equation is:

$$\frac{\partial}{\partial \bar{x}}\left(\bar{h}^3\frac{\partial \bar{P}}{\partial \bar{x}}\right)+\pi^2\left(\frac{D}{L}\right)^2\frac{\partial}{\partial \bar{y}}\left(\bar{h}^3\frac{\partial \bar{P}}{\partial \bar{y}}\right)=6\frac{\partial \bar{h}}{\partial \bar{X}} \quad (2)$$

Dimensionless parameters in this equation are as follows:

$$\bar{x}=\frac{x}{\pi D};\ \bar{y}=\frac{y}{L};\bar{h}=\frac{h}{h_2};\bar{P}=\frac{P}{P_{ref}};$$

$$P_{ref}=\mu\pi DU/h_2^2$$

This is a partial differential equation which does not have a closed-form solution. Analytical solutionsare only available for extreme cases such as the infinitely long approximation (ILA) and infinitely short approximation (ISA).In this paper, the analytical solution of Naffin (2009)is presented.

2.1.1. InfinitelyLong Approximation Bearing (ILA)

If $L >> D$, it can be said that $(D/L)^2 << 1$ and neglect the second term of the left hand side of Eq. (2). Physically, it means that one can ignore the side leakage term of the bearing. This approximation is acceptable for$L/D \geq 3$. Using this assumption and letting $x = R\theta$,$U = R\omega$,$h = C(1 + \varepsilon \cos\theta)$Eq. (3)is obtained:

$$\frac{dP}{dx} = 6\mu\omega\left(\frac{R}{C}\right)^2\left[\frac{1}{(1+\varepsilon\cos\theta)^2} - \frac{h_m}{C(1+\varepsilon\cos\theta)^3}\right] \quad (3)$$

Whereh_m is the value of the fluid film thickness at the location in which maximum pressure occurs. Finally, the pressure distribution in this case is:

$$P = \frac{6\varepsilon\sin\theta(2+\varepsilon\cos\theta)}{(2+\varepsilon^2)(1+\varepsilon\cos\theta)^2}\mu\omega\left(\frac{R}{C}\right)^2 \quad (4)$$

By applying the half-Sommerfeld boundary condition, the value of Sommerfeld number in terms of the eccentricity value is (5):

$$S = \frac{(2+\varepsilon^2)(1-\varepsilon^2)}{6\pi\varepsilon}\left[\frac{1}{\pi^2(1-\varepsilon^2)+4\varepsilon^2}\right] \quad (5)$$

In this case, load-bearing capacity is obtained using Eq. (6):

$$W = \frac{3\omega\mu LD^3}{4C^2}\frac{\varepsilon(4\varepsilon^2+\pi^2-\pi^2\varepsilon^2)}{(2+\varepsilon^2)(1-\varepsilon^2)} \quad (6)$$

2.1.2. Infinitely Short Approximation Bearing (ISA):

If$L << D$, it can be said$(D/L)^2 >> 1$ and one can neglect the circumferential component of flow compared to the side leakage flow. This approximation represents acceptable solutions for$L/D < 0.25$. By disregarding the second term of Eq. (2)and letting$x = R\theta,\ dh/d\theta = -C\varepsilon\sin\theta/R$, pressure distribution is obtained using the following Eq.(7):

$$P = \frac{3\mu U}{C^2R}\left(\frac{L^2}{4} - y^2\right)\frac{\varepsilon\sin\theta}{(1+\varepsilon\cos\theta)^3} \quad (7)$$

Using half-Sommerfeld boundary conditions, the relation of Sommerfeld number with the eccentricity value is:

$$S = \frac{(1-\varepsilon^2)^2}{\pi\varepsilon[\pi^2(1-\varepsilon^2)+16\varepsilon^2]^{1/2}}\left(\frac{D}{L}\right)^2 \quad (8)$$

Load capacity for this case is obtained from the Eq.(9):

$$W = \frac{\mu D\omega L^3}{8C^2}\frac{\pi\varepsilon}{(1-\varepsilon^2)^2}(0.62\varepsilon^2)^{\frac{1}{2}} \quad (9)$$

2.1.3.Finite Length Bearing:

In this section, the purpose is to obtain the model for bearings without dimensional limitation that connects the eccentricity and load capacity according to Eqs. (6) and (9). By the definition of dimensionless parameter as follows and substituting in Eqs. (6) and (9) one obtains the Eqs.(11) and (12).

$$\bar{W} = \frac{C^2}{\mu D^4\omega}W \quad (10)$$

$$\bar{W} = \frac{3\varepsilon(4\varepsilon^2+\pi^2-\pi^2\varepsilon^2)^{\frac{1}{2}}}{4(2+\varepsilon^2)(1-\varepsilon^2)}\left(\frac{L}{D}\right);$$

$$\frac{L}{D} \geq 3.0 \quad (11)$$

$$\bar{W} = \frac{\pi\varepsilon}{8(1-\varepsilon^2)^2}(0.62\varepsilon^2+1)^{\frac{1}{2}}\left(\frac{L}{D}\right)^3;$$

$$\frac{L}{D} < \frac{1}{4} (12)$$

The Eqs.(11)and(12) can be written as:

$$\bar{W} = [f_L(\varepsilon)]\left(\frac{L}{D}\right)\frac{L}{D} \geq 3.0 (13)$$

$$\bar{W} = [f_S(\varepsilon)]\left(\frac{L}{D}\right)^3\frac{L}{D} < \frac{1}{4} \quad (14)$$

By taking the logarithm of both sides of these equations:

$$\log\bar{W} = \log[f_L(\varepsilon)] + \log\left(\frac{L}{D}\right);\ \frac{L}{D} \geq 3.0 \quad (15)$$

$$\log\bar{W} = \log[f_S(\varepsilon)] + 3\log\left(\frac{L}{D}\right);\frac{L}{D} < \frac{1}{4} \quad (16)$$

Eqs. (15) and (16), linearly relates $\log(\bar{W})$ and $\log(L/D)$. The general form of proposed relation is as follows:

$$Y = f(\varepsilon, X)\ \frac{1}{4} < \frac{L}{D} < 3 \quad (17)$$

Where in this equation is$Y = \log(\bar{W})$ and$X = \log(L/D)$. Equations for short and long bearing can be written similar to Eq. (17). In this case, one can write Eqs. (15) and (16) in the form of Eq. (18) and (19):

$$Y = A_S + 3X \qquad \frac{L}{D} < \frac{1}{4} \quad (18)$$

$$Y = A_L + X \qquad \frac{L}{D} \geq 3.0 \quad (19)$$

Where $A_S = \log[f_S(\varepsilon)]$ and $A_L = \log[f_L(\varepsilon)]$. Equation (17) may now be anchored long and short bearing models in this form. The lower and upper matching points are $X_S = \log\left(\frac{1}{4}\right)$and $X_L = \log$ (3), respectively. The Eqs. (17) and (18) correspond in$X = X_S$. Similarly, when$X = X_L$ *Eq*s. (17) and (19) match. Additionally, the slope of the curves must be equal at the connection point. Therefore, the boundary conditions for connecting the finite and short bearing model are:

$$f(\varepsilon, X_S) = A_S + 3X_S \quad (20)$$

$$\frac{df(\varepsilon,X)}{dX}\Big|_{X=X_S} = 3 \quad (21)$$

For connecting the finite and long bearing model, the boundary conditions are:

$$f(\varepsilon, X_L) = A_L + X_L \quad (22)$$

$$\frac{df(\varepsilon,X)}{dX}\Big|_{X=X_L} = 1 \quad (23)$$

Hence, there are four boundary conditions. For obtaining a smooth curve, Eq. (17)is written in the form of a third order polynomial:

$$Y = f(\varepsilon, X) = C_3X^3 + C_2X^2 + C_1X + C_0 \frac{1}{4} \leq \frac{L}{D} \leq 3 \quad (24)$$

The unknown coefficients are obtained as:

$$C_3 = \frac{G_1}{G_2} \quad (25)$$

$$G_1 = A_S + 3X_S - (A_L + X_L) + 3X_L - X_S - \left(\frac{-2}{2(X_L - X_S)}\right)\left({X_S}^2 - {X_L}^2\right) \quad (26)$$

$$G_2 = {X_S}^3 - {X_L}^3 + \left(\frac{3{X_S}^4 + 3{X_L}^4}{2(X_L - X_S)}\right) - \left(\frac{6{X_L}^2{X_S}^2}{2(X_L - X_S)}\right) + 3{X_S}^2X_L - 3{X_L}^2X_S \quad (27)$$

$$C_2 = \frac{-2-3C_3{X_L}^2+3C_3{X_S}^2}{2(X_L-X_S)} \quad (28)$$

$$C_1 = 3 - 3C_3{X_S}^2 - 2C_2X_S \quad (29)$$

$$C_0 = A_L + X_L - C_3{X_L}^3 - C_2{X_L}^2 - C_1X_L \quad (30)$$

In these equations:

$$X_S = \log\left(\frac{1}{8}\right) \quad , \quad X_L = \log(4.75)$$

$$A_L = \log\left(f_L(\varepsilon)\right) = \log\left[\frac{3\varepsilon(4\varepsilon^2+\pi^2-\pi^2\varepsilon^2)^{\frac{1}{2}}}{4(2+\varepsilon^2)(1-\varepsilon^2)}\right] \quad (31)$$

$$A_S = \log\left(f_S(\varepsilon)\right) = \log\left[\frac{\pi\varepsilon}{8(1-\varepsilon^2)^2}\left(0.62\varepsilon^2 + 1\right)^{\frac{1}{2}}\right] \quad (32)$$

This model is solved using short bearing model (Eq. (18)) when$X < X_S$. Similarly, when$X > X_L$, it is solved using the long bearing model (Eq. (19)). The error of the methodis about 56% compared to the given data in Khonsari and Booser (2008) which is a significant error. If the lower match point (X_S) is 0.125 and upper match point (X_L) is 4.75, the maximum error reduces to about 14%. In this case, with increasing the load or eccentricity, the error grows exponentially for a relatively short bearing. One can improve the growth of short bearing error by changing the eccentricity term ($f_S(\varepsilon)$) in load-dimensionless equation.

Short bearing error where$\varepsilon = 0.1$ will exponentially grow with increasing the load or eccentricity. So, the $f_S(\varepsilon)$term must be modified by an exponential correction factor $C_S(\varepsilon)$:

$$f_s = C_s\left(\varepsilon\right)\frac{\pi\varepsilon}{8\left(1-\varepsilon^2\right)^2}\left(0.62\varepsilon^2+1\right)^{\frac{1}{2}} = \left(1-A\left(\varepsilon-0.1\right)^B\right)\frac{\pi\varepsilon}{8\left(1-\varepsilon^2\right)^2}\left(0.62\varepsilon^2+1\right)^{\frac{1}{2}} \quad (33)$$

By taking the logarithm of Eq. (33), the term As in Eq.(32) is modified as:

$$A_S = \log[(1 - A(\varepsilon - 0.1)^B)\frac{\pi}{8(1-\varepsilon^2)^2} \times (0.62\varepsilon^2 + 1)^{\frac{1}{2}}] \quad (34)$$

The coefficients A and B are achieved using trial-and-error for minimum error:

$$A = 0.7 \quad , \quad B = 10$$

$$A_s = \log[1 - 0.7(\varepsilon - 0.1)^{10}\frac{\pi\varepsilon}{8(1-\varepsilon^2)^2} (0.62\varepsilon^2 + 1)^{\frac{1}{2}}] \quad (35)$$

Similarly, long bearing error can be reduced by multiplying a linear coefficient in As:

$$A_L = \log\left[(0.91 + 0.19\varepsilon)\frac{3\varepsilon(4\varepsilon^2 + \pi^2 - \pi^2\varepsilon^2)^{1/2}}{4(2+\varepsilon^2)(1-\varepsilon^2)}\right] \quad (36)$$

The maximum error of this model is 5.8% which compared to 13.7% in the previous model has considerably reduced (Naffin (2009). This model is thus believed to be appropriate to determine load-bearing capacity. The eccentricity ratio is obtained using a computer program.

2.2. Dynamic Mesh Method

For most CFD simulations, the physical geometry does not change with time, and a fixed mesh will then generally be the appropriate choice. For deforming geometries, dynamic meshing becomes a necessary part of the modeling (Fluent (2009). Dynamic mesh method is used when the shape of fluid domain changes as a result of moving boundaries Gertzos *et al.* (2008). There are several methods for mesh deformation in which following methods are commonly used:

- Smoothing methods
- Dynamic layering
- Remeshing methods

Smoothing method itself is categorized to several types. In this research, the Diffusion-Based smoothing method has been used. In the diffusion-based smoothing, the mesh deformation is governed by the diffusion Eq.

$$\nabla.(\gamma\nabla\bar{u}) = 0 \quad (37)$$

In this equation,$\bar{u}$ is the mesh displacement velocity. For this equation, boundary conditions are usually determined according to the moving boundaries. Then, the Laplace Eq. (37) specifies the propagation of boundaries displacement in internal nodes of the transformed mesh. Diffusion coefficient γ in Eq. (37) is used to control the effect of moving boundaries on internal nodes. The computational cost of diffusion-based smoothing is higher than

other smoothing methods. The advantage of this method is that it maintains the best mesh quality and allows greater deformation of the boundaries without mesh rupturing. It should be noted that with the diffusion-based smoothing, the interior mesh motion is governed by the solution of Eq. (37) and the prescribed boundary motion, and not by mesh irregularities. Poor quality elements or mesh defects cannot be smoothed by this method, but rather move together with the pre-computed (at the beginning of each mesh update) displacement velocity $\bar{u}$ (Fluent (2009).

According to Fig. 3, in the first step of numerical method, primary geometry is produced. After that a special mesh is provided from this geometry. Then the oil flow in bearing is analyzed by solving the equations of continuity (Eq. (38)), momentum (Eq. (39)) and energy (Eq. (40)) simultaneously. A pressure distribution is gained from this analysis and by putting the force caused by this pressure distribution (F_{Aero}) to dynamic equations (Eq. (41)), the acceleration of journal is calculated. Solving Kinematic equations (Eqs. (42) and (43)) leads to evaluating the value of velocity and location of journal. By calculating the difference between this location and prior location the value of displacement is calculable. If displacement has a non-negligible value, a new geometry with new location of journal is produced and the procedure will be prepared till reaching to a negligible value for displacement.

$$\frac{\partial \rho}{\partial t}+\frac{\partial}{\partial x_i}(\rho \mathrm{u}_i)=0 \tag{38}$$

$$\frac{\partial}{\partial t}(\rho u_i)+\frac{\partial}{\partial x_i}(\rho \mathrm{u}_i \mathrm{u}_j)=-\frac{\partial P}{\partial x_i}+\frac{\partial \tau_{ij}}{\partial x_j} \tag{39}$$

$$\frac{\partial}{\partial t}(\rho h_{tot})+\frac{\partial}{\partial x_j}(\rho h_{tot}\,\mathrm{u}_j)=\frac{\partial P}{\partial t} + \frac{\partial}{\partial x_j}(\mathrm{u}_i \tau_{ij}+\lambda \frac{\partial T}{\partial x_j}) \;;\; h_{tot}=h+\frac{1}{2}u_i^2 \tag{40}$$

$$mg+F_{Aero}=m\ddot{s} \tag{41}$$

$$\dot{s}=\dot{s}_0+\ddot{s}t \tag{42}$$

$$s=s_0+\dot{s}t \tag{43}$$

3. NUMERICAL SIMULATION

Geometry: The proposed geometry is the space between the two cylinders that are initially concentric but, during the simulation, the inner cylinder becomes eccentric. The inner cylinder is considered as a rigid body that can move due to pressure distribution from fluid flow applied to its surface. The dynamic and cinematic equations of motion are applied to the inner cylinder to obtain its eccentricity. Thus, the space between the outer and inner cylinder is deformed during the simulation. Due to the symmetry of the problem and to save time, one half of the bearing is simulated (Fig.4).

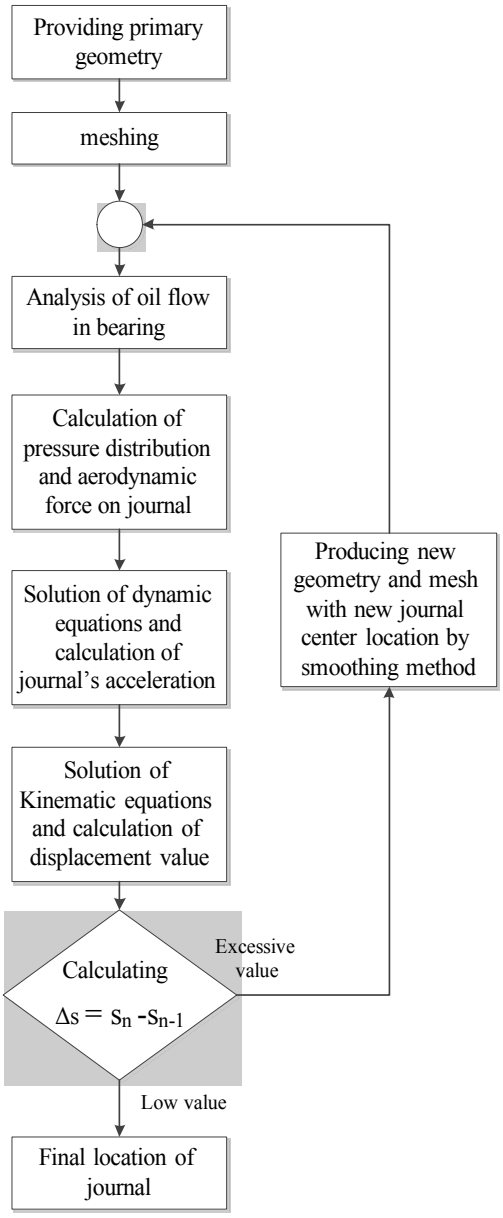

Fig. 3. Numerical solution process.

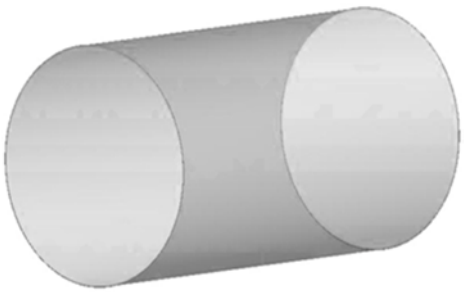

Fig. 4. Long bearing geometry.

Generated mesh: For the simulation, a structured grid is generated. To evaluate the grid independency of the simulation, several grid sizes are used for the eccentricity value of 0.3 and then, the obtained maximum pressures as shown in Fig.5 are compared. According to this figure, the grid independency is satisfied at 86400 cells in which the number of divisions in the radial, axial and circumferential direction is 12, 30 and 240, respectively (Fig.6). Due to the change of the geometry between the two cylinders during the simulation, the grid deformation is obtained by the dynamic mesh method.

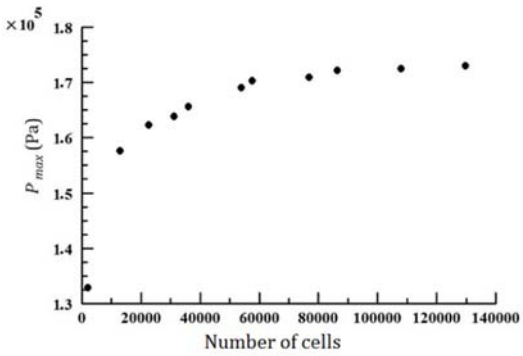

Fig. 5. Mesh study diagram.

Fig. 6. Generated mesh for long bearing.

Boundary conditions: Simulations are performed under light, medium and heavy loads. Rotational speed of the journal is 600 rpm for all the cases. Reynolds number is obtained from the following relation:

$$Re = \frac{\rho UC}{\mu} = 15.65$$

The flow regime is always laminar and unsteady. In all simulations, the time step is 0.00005 seconds and the number of iterations per time step is 50. To determine the effect of applied load, a rigid body which has a weight equal to the applied load is modeled at the place of inner cylinder. The mass of rigid body for each case is reported in table 1.

Boundary conditions according to Fig.7 are as follow:

(1) Symmetry plane: to save time and due to the symmetry conditions, the symmetry boundary condition has been used. The mesh in this plane is allowed to be deformed

(2) Left plane: opening boundary condition is applied to this plane. Similar to the symmetry plane, the mesh in this plane is allowed to be deformed.

(3) Outer cylinder: The outer cylinder is modeled as the stationary wall boundary condition.

(4) Inner cylinder: For the inner cylinder, the moving wall boundary condition is considered. This wall rotates with a rotational speed of 600 rpm. Imbalance between the integral of pressure distribution and the load which are applied to the inner cylinder causes the inner cylinder to move. The inner cylinder moves such that these two forces neutralize each other.

Table 1 The mass of rigid body at different loading

	Sommerfeld Number	Rigid Body Mass
Long Bearing	0.1	125.2505 kg
	0.06	208.7508 kg
	0.035	357.8586 kg
Short Bearing	5	0.1566 kg
	2	0.3914 kg
	1	0.7813 kg
Finite Bearing	0.65	4.8173 kg
	0.19	16.4803 kg
	0.06	52.1877 kg

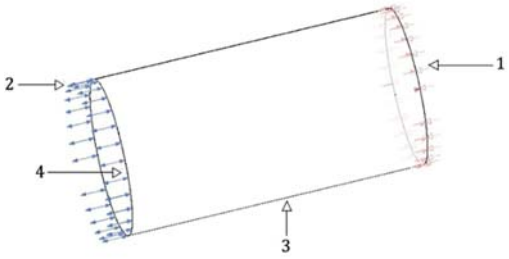

Fig. 7. Long bearing boundary condition.

4. DYNAMIC MESH VERIFICATION

4.1. ILA Case

For infinitely long bearing case, the values of the eccentricity under different loads are obtained by dynamic mesh method as well as the analytical method which are then compared to each other in Fig.8. Maximum error is below 7%.

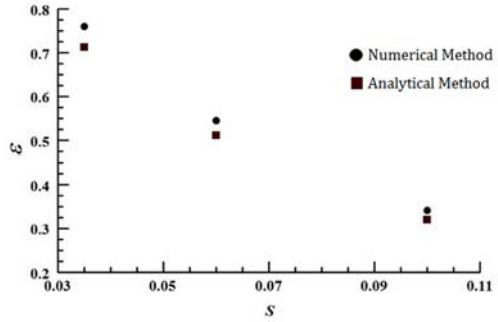

Fig. 8. The value of eccentricity ratio for different Sommerfeld numbers for long bearing

Figure 9 shows the obtained pressure distribution from the analytical and numerical solution for the infinitely long bearing under different loads. With increasing S, the pressure distribution changes in a way that the minimum and maximum pressures approach to each other. It's obvious that the obtained numerical pressure distribution has an appropriate adaptation to the analytical method especially in light loading.

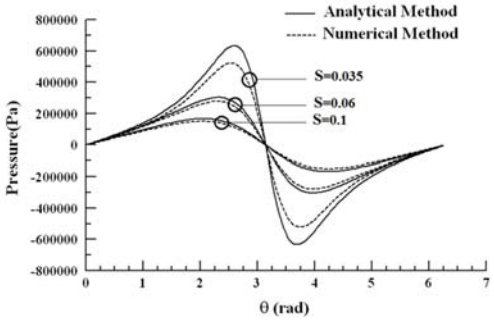

Fig. 9. The pressure distribution obtained by both method at different loads in long bearing.

4.2. ISA Case

Figure 10 compares the value of eccentricity obtained from the analytical and the dynamic mesh method under different loads. The pressure distribution of the analytical and the dynamic mesh method are illustrated in Fig. 11 and Fig. 12, respectively.

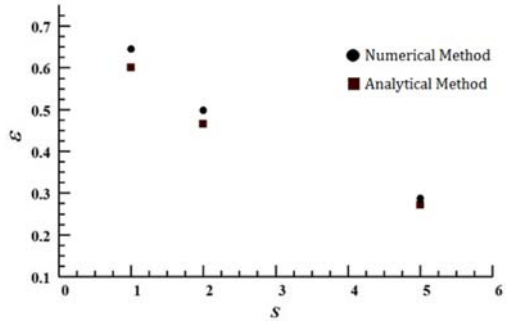

Fig. 10. Eccentricity ratio vs. Sommerfeld number for short bearing.

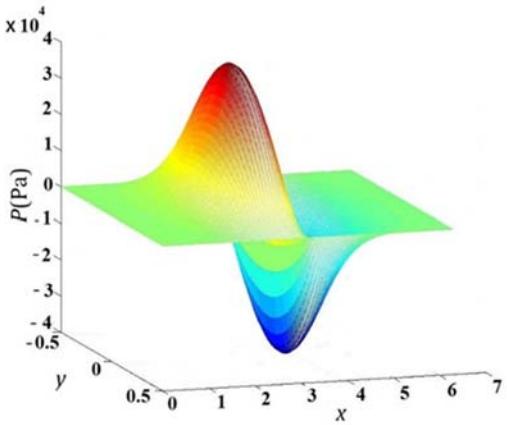

Fig. 11. The pressure distribution obtained by analytical solution in short bearing.

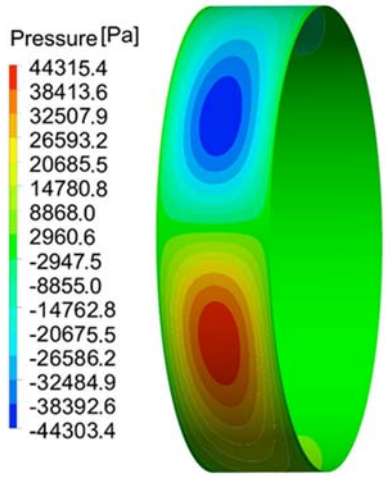

Fig. 12. The pressure distribution obtained by dynamic mesh solution in short bearing.

4.3. Finite Length Case

Figure 13 shows the value of eccentricity for a finite length bearing obtained from the dynamic mesh method and the analytical method. It can be observed that the numerical method based on the dynamic mesh has a suitable accuracy for analysing the journal bearings.

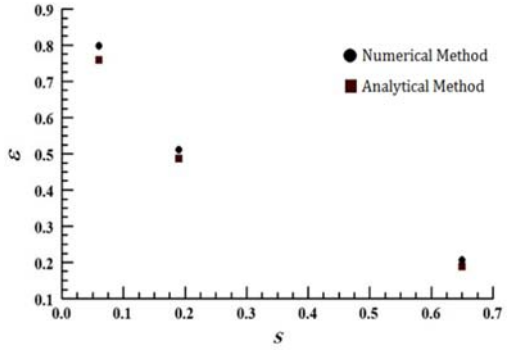

Fig. 13. Eccentricity ratio vs. Sommerfeld numbers for finite bearing.

5. ANALYSIS OF TURBOCHARGER'S BEARING

Turbocharger's bearing consists of four input holes for appropriate lubrication. The weight of the turbine and compressor is carried by two journal bearings. Effect of rotational speed on the eccentricity ratio, attitude angle, maximum temperature of the bearing, average temperature of oil output, leakage flow, and friction torque is studied. Three different rotational speeds are investigated. Then, a turbocharger's bearing with four axial grooves are simulated. Fig. 14 shows the simulated geometry.

Fig. 14. The simulated geometry.

5.1. Bearing's Geometry

The dimensions of proposed bearing are as follow Deligant*et al.* (2011):

Bearing length:	$L = 3.8$ mm
Bearing diameter:	$D = 7$ mm
Clearance:	$C = 15$ μm
Applied load from the turbine and compressor:	$W = 0.564$ N
The diameter of oil input holes:	$D_i = 1.4$ mm

5.2. Lubricant Characteristics

In the simulation, the oil HC 5W-30 is used. The characteristics of the oil are as follow Schmidt*et al.* (2006):

Density: The oil's density variation with temperature is obtained using Eq. (44):

$$\rho = -0.625T + 1032.5 \quad (44)$$

Where$\rho$is density in kg / m^{3}and T is absolute temperature.

Viscosity: Eq. (45)represents the changes of viscosity with temperature:

$$\mu = ae^{\frac{b}{T-c}}, \quad a = 7.48 \times 10^{-5}, \quad b = 1005.2, \; c = 157.45 \quad (45)$$

Where μ is viscosity in Pa.s.

Heat capacity: Heat capacity of the lubricant varies with temperature according to Eq. (46):

$$C_P = 3.84T + 873.076 \quad (46)$$

C_P is specific heat capacity in J/kg K.

5.3 Generated Mesh

In this simulation, similar to the plain bearing case, the generated mesh, shown in Fig. 15, consists of 86400 cells.

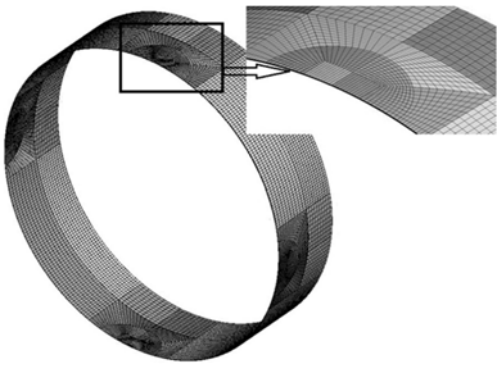

Fig. 15. Generated mesh for turbocharger bearing.

5.4. BoundaryConditions

The boundary conditions according to Fig. 16 are as:

(1) Pressure inlet boundary condition is used at the input holes of the bearing.Relative pressure value at the input is5 bar and input oil temperature is 323 K. Stationary condition is used to consider mesh deformation.

(2) Pressure outlet boundary condition is applied to the right hand section of the bearing. Relative pressure value is zero. The mesh in this plane is allowed to be deformed.

(3) In the symmetry plane of the bearing, the symmetry boundary condition is used. Such as the outlet section, the symmetry plane mesh is allowed to be deformed.

(4) Bearing shell is considered as the stationary wall boundary condition. Stationary condition has been used to consider the mesh movement.

(5) Moving wall boundary condition is applied to the inner cylinder of the bearing. Rigid body boundary condition has been intended to the mesh movement on this cylinder.

The variation of eccentricity as a function of rotational speed is shown in Fig. 17. As the rotational speed increases, the Sommerfeld number increases. Increase of the Sommerfeld number means decrease of load and consequently decrease

of eccentricity.

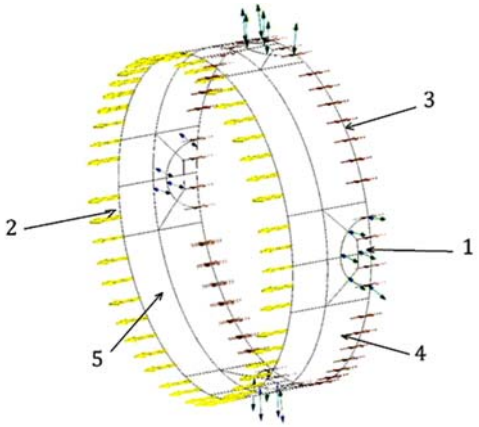

Fig. 16. Boundary condition in turbocharger's bearing simulation.

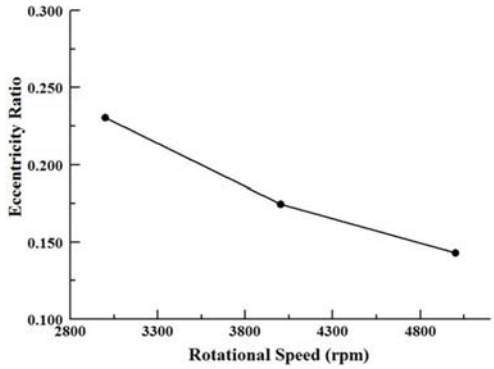

Fig. 17. Changes of eccentricity ratio vs. rotational speed of the journal.

The effect of rotational speed on the attitude angle is illustrated in Fig. 18. Increasing the rotational speed of the journal causes the attitude angle to decrease. Increasing the rotational speed leads to an increase in the Sommerfeld number and thus, reduction of the growing rate of attitude angleKhonsari and Booser (2008). In further analyses of turbocharger's bearings, at high rotational speeds, the attitude angle approaches to 90(Deligant *et al.* (2011);Deligant *et al.* (2011; Deligant *et al.* (2009).

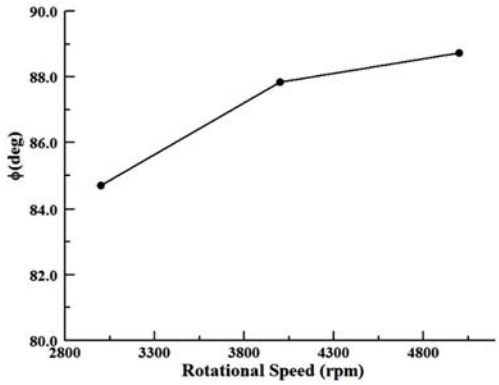

Fig. 18. Changes of the attitude angle vs. rotational speed of the journal.

As shown in Fig. 19, the rotational speed of the journal has relatively small effect on the oil flow rate. It has been experimentally shown in the literatureNaffin (2009; Schmidt *et al.* (2006).

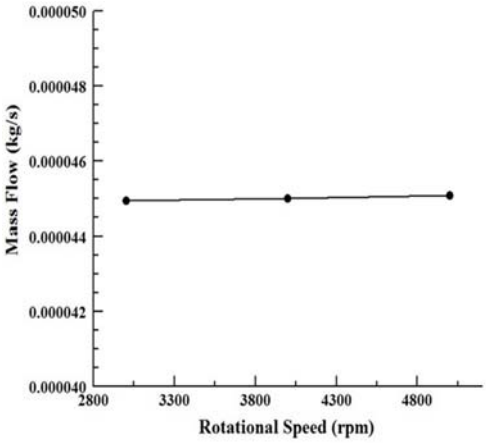

Fig. 19. Changes of the leakage flow in rotational speed of the journal.

Obtained temperature distribution is shown in Fig.20. Away from the input holes in the direction of rotation, the oil temperature increases and after arriving at the next hole in which the lubricant mixes with the fresh input oil, it drops. The temperature rise due to the eccentricity of the shaft is high at its right half. Fig. 21 plots the maximum oil temperature occurring in the bearing versus the rotational speed. As expected, due to the friction losses, increasing the rotational speed has a direct effect on the maximum temperature and consequently the outlet average temperature.

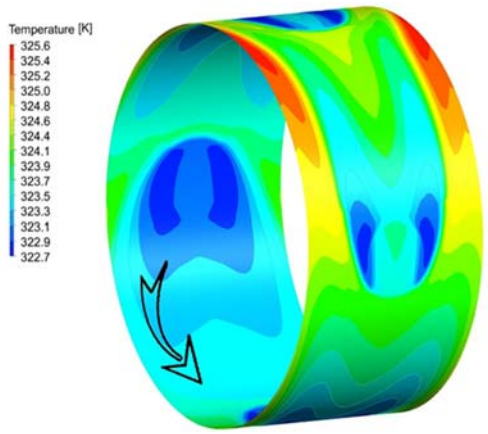

Fig. 20. Oil temperature distribution in the speed of 400 rpm.

Figure 22 shows the effect of the rotational speed on the frictional torque. Increasing the speed has a direct effect on the frictional losses. This result has been experimentally obtained by Deligant *et al.* (2012). With increasing the rotational speed, velocity gradient and consequently shear stress increase. Increasing the shear stress leads to an increase in the friction torque.

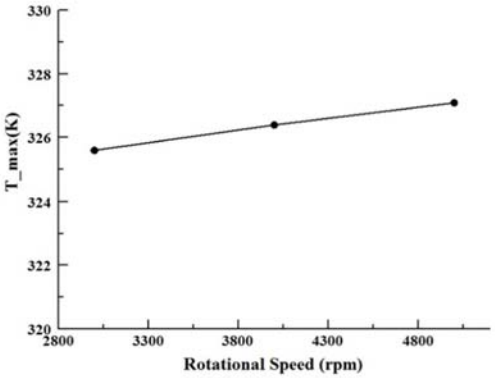

Fig. 21. Changes of the maximum temperature in rotational speed of the journal.

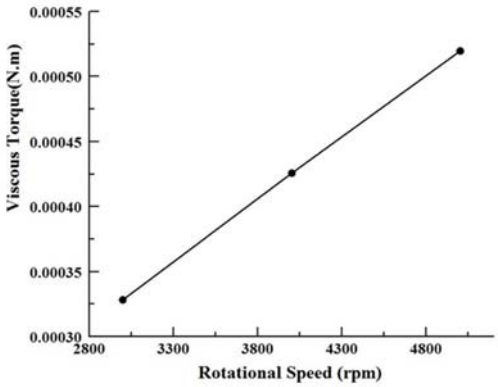

Fig. 22. Changes of frictional in rotational speed of the journal.

5.6. Considering the Effects of Adding Axial Grooves:

In this section the effect of adding an axial groove to the bearing is studied. Groove dimensions are chosen as follow Deligant *et al.* (2009; Khonsari and Booser (2008):

Groove length: $L = 3$ mm

Groove width: $W = 0.8$ mm

Groove deep: $H = 0.25$ mm

In order to simulate a bearing with an axial groove, a structured mesh which consists of 146000 cellsis generated (Fig. 23).The number of division in the direction of fluid film and circumferential direction in this case are the same as divisions' number which obtained by mesh study. The simulation has been performed for 3000 rpm.

In table 2, the results of simulating the performance of a grooved bearing are compared to a non-grooved bearing. The results indicate a 20% increase in eccentricity and a 24% decrease in attitude angle by adding grooves. The chamber of turbine has a relatively high temperature. The best way to cool the shaft is to increase the oil flow. This requires increasing the input pressure which on the other hand, leads to problems such as increase in pressure of lubrication duct and seals damaging. The results in table 2 indicate a 3.8 fold increase of oil flow as a result of groove use. It is clear that total pressure drops from input to output in non-grooved bearings due to the very small distance between the journal and shell. Addition of axial grooves leads to an increased clearance of the bearing and therefore, the reduced pressure drops and the flow rate increases. The rate of temperature rise due to the frictional losses is significantly reduced and this is due to the increase of oil mass flow. The frictional torque has reduced 5%which is another advantage of the axial grooved bearing. In Fig. 24, Fig. 25 and Fig. 26 temperature distribution, pressure distribution, and change in the position of the journal in different time steps are shown, respectively.

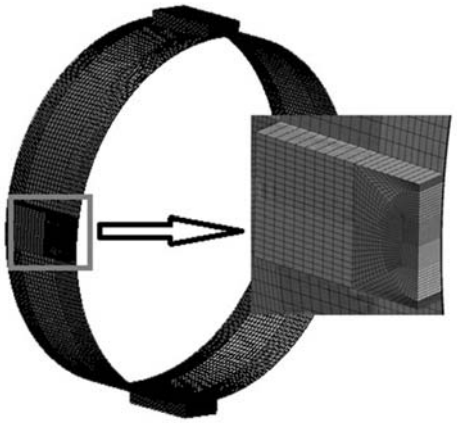

Fig. 23. Generated mesh for turbocharger bearing with axial groove.

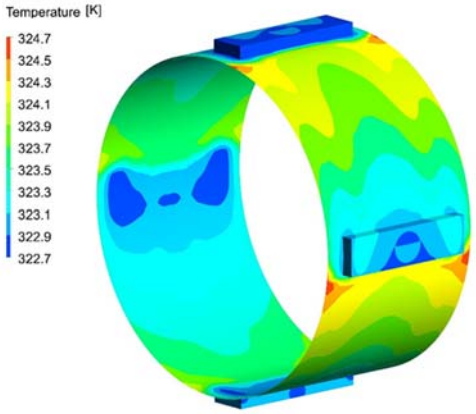

Fig. 24. Temperature distribution in bearing with axial grooves.

6. CONCLUSION

In this paper a comprehensive method for the analysis of journal bearings based on the dynamic mesh method is presented. In order to show the validity of this method, three different cases for which the analytical solutions exists have been simulated. These cases are infinitely long bearing, infinitely short bearing, and finite bearing. The

Table 2 The comparison between simulation of bearing with four axial grooves and bearing without groove

	e	∅[deg]	ΔT_{max}[K]	ΔT_{ave}[K]	Mass flow[kg/ m^3]	Viscous Torque [N m]
without grooves	0.1936	83.4832	3.1	2.185	2.82611e-005	3.3935e-04
With grooves	0.2381	63.1236	1.7	0.665	10.7845 e-005	3.2221e-04
values of difference	22%	-24%	- 82%	-228%	282%	-5%

results reveal an acceptable agreement between the dynamic mesh method and the analytical solution. The difference between the results from the dynamic mesh method and the analytical method for the infinitely long bearing is lower than the other two cases.

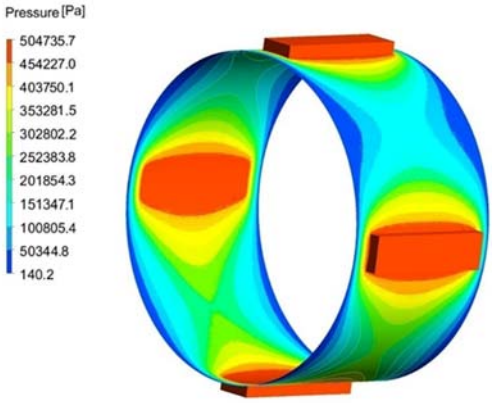

Fig. 25. Pressure distribution in bearing with axial grooves.

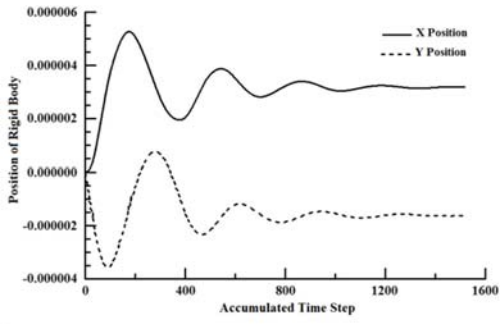

Fig. 26. Position of X and Y axes at different time steps.

In the simulation of turbocharger's bearing, it was observed that increasing the rotational speed of the shaft results in a decrease in the eccentricity and the attitude angle of the journal while the temperature rise resulted from frictional losses and also frictional torque increases. The leakage flow is increased with increasing the rotational speed of the journal. Adding the axial grooves to turbocharger's bearing leads to an increase inthe eccentricity and reduction in the attitude angle. Lubricant leakage flow is more in grooved bearing compared to simple bearing. Adding the axial grooves reduces the lubricant temperature rise.

REFERENCES

Chauhan, A., *et al*. (2014). CFD Based Thermo-Hydrodynamic Analysis of Circular Journal Bearing. *Journal of Advanced Mechanical Engineering* 4(5), 475-482.

Christopherson, D. G. (1941). A new mathematical method for the solution of film lubrication problems. *Proceedings of the Institution of Mechanical Engineers* 146(1), 126-135.

Deligant, M., P. Podevin and G. Descombes (2011). CFD model for turbocharger journal bearing performances. *Applied Thermal Engineering* 31(5), 811-819.

Deligant, M., P. Podevin and G. Descombes (2012). Experimental identification of turbocharger mechanical friction losses. *Energy* 39(1), 388-394.

Deligant, M., *et al*. (2009). 3D Thermal Steady-State CFD Analysis of Power Friction Losses in a Turbocharger's Journal Bearing and Comparison With Finite Difference Method and Experimentation: Bratislava.

Dubois, G. B. and F. W. Ocvirk (1953).*Analytical derivation and experimental evaluation of short-bearing approximation for full journal bearings*: US Government Printing Office.

Dumont, K., *et al*. (2004). Validation of a fluid–structure interaction model of a heart valve using the dynamic mesh method in fluent. *Computer methods in biomechanics and biomedical engineering* 7(3), 139-146.

Fluent, INC (2009) Fluent 12.1. 4 Documentation. *User's guide*.

Gao, G., *et al*. (2014). Numerical analysis of plain journal bearing under hydrodynamic lubrication by water. *Tribology International* 75, 31-38.

Gao, G., *et al*. (2015). CFD analysis of load-carrying capacity of hydrodynamic lubrication on a water-lubricated journal bearing. *Industrial Lubrication and Tribology* 67(1), 30-37.

Gertzos, K. P., P. G. Nikolakopoulos and C. A. Papadopoulos (2008). CFD analysis of journal bearing hydrodynamic lubrication by Bingham lubricant. *Tribology International* 41(12), 1190-1204.

Gümbel, L. (1921). Verleich der Ergebnisse der

rechnerischen Behandlung des Lagerschmierungsproblem mit neueren Versuchsergebnissen. *Mbl. berl. Bez.(VDI)*, 125-128.

Khonsari, M. M. and E. Richard Booser (2008).*Applied tribology: bearing design and lubrication*. 12.

Kumar, S. C. and R. Ganapathi (2015). CFD Analysis on Hydrodynamic Plain Journal Bearing using Fluid Structure Interaction Technique. International Journal of Engineering Research and Technology 4. ESRSA Publications.

Lin, Q., *et al*. (2013). Analysis on the lubrication performances of journal bearing system using computational fluid dynamics and fluid–structure interaction considering thermal influence and cavitation. *Tribology International* 64, 8-15.

Naffin, R. K. (2009).*Development of an Analytical Design Tool for Journal Bearings*, The Pennsylvania State University.

Naïmi, S., M. Chouchane and J. L. Ligier (2010). Steady state analysis of a hydrodynamic short bearing supplied with a circumferential groove. *Comptes Rendus Mecanique* 338(6), 338-349.

Pai, R., D. J. Hargreaves and R. Brown (2001). Modelling of fluid flow in a 3-axial groove water bearing using computational fluid dynamics. 14th Australian fluid Mechanics conference.

Raimondi, A. A. and J. Boyd (1958). A Solution for the Finite Journal Bearing and its Application to Analysis and Design: I. *ASLE Transactions* 1(1), 159-174.

Reynolds, O. (1886). On the Theory of Lubrication and Its Application to Mr. Beauchamp Tower's Experiments, Including an Experimental Determination of the Viscosity of Olive Oil. *Proceedings of the Royal Society of London* 40(242-245), 191-203.

Schmidt, R., G. Klingenberg and M. Woydt (2006). New lubrication concepts for environmental friendly machines. BAM Research Report.

Shigley, J. (2003). Mechanical engineering design.

Sommerfeld, A. (1904). Zur hydrodynamischen theorie der schmiermittelreibung. *Z. Math. Phys* 50(97), 155.

Tao, W., *et al*. (2003). 2003-01-0924 CFD Simulation of Connecting Rod Bearing Lubrication. *SAE SP*, 169-174.

Wu, W., *et al*. (2015). Application of CFD to model oil–air flow in a grooved two-disc system. *International Journal of Heat and Mass Transfer* 91, 293-301.

Zhang, H., Y. R. Xu and H. P. Cai (2010). Using CFD software to calculate hydrodynamic coefficients. *Journal of Marine Science and Application* 9(2), 149-155.